DISCLAIMER

This report was prepared as an account of work sponsored by an agency of the United States Government. Neither the United States Government nor any agency thereof, nor any of their employees, makes any warranty, express or implied, or assumes any legal liability or responsibility for the accuracy, completeness, or usefulness of any information, apparatus, product, or process disclosed, or represents that its use would not infringe privately owned rights. Reference herein to any specific commercial product, process, or service by trade name, trademark, manufacturer, or otherwise does not necessarily constitute or imply its endorsement, recommendation, or favoring by the United States Government or any agency thereof. The views and opinions of authors expressed herein do not necessarily state or reflect those of the United States Government or any agency thereof. Reference herein to any social initiative (including but not limited to Diversity, Equity, and Inclusion (DEI); Community Benefits Plans (CBP); Justice 40; etc.) is made by the Author independent of any current requirement by the United States Government and does not constitute or imply endorsement, recommendation, or support by the United States Government or any agency thereof.

NATIONAL ENERGY TECHNOLOGY LABORATORY

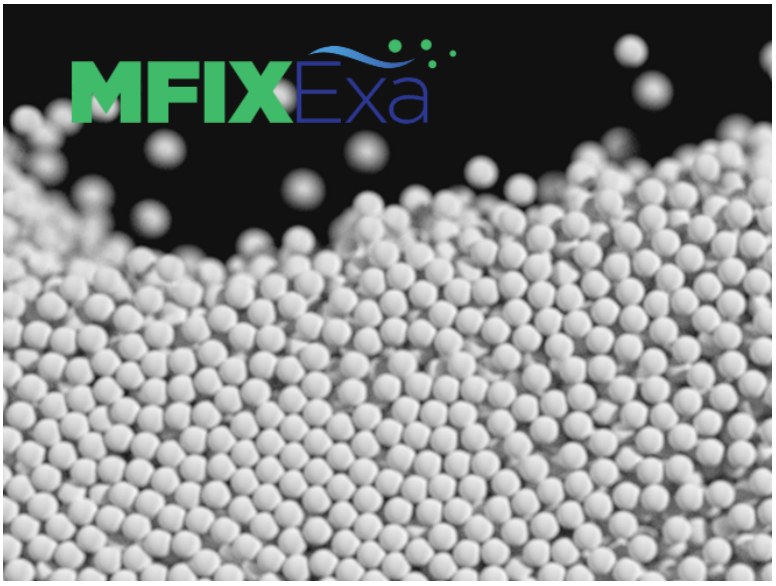

Small-scale validation tests for MFIX-Exa CFD-DEM

September 24, 2025

U.S. DEPARTMENT of ENERGY | NATIONAL ENERGY TECHNOLOGY LABORATORY

Office of Fossil Energy and Carbon Management
DOE/NETL-2025/4951

Disclaimer

Cover Illustration:
CFD-DEM simulation of a fluidized bed rendered with Blender courtesy of Justin Weber.

Keywords:
MFIX-Exa, AMReX, CFD-DEM, validation

Suggested Citation:
Fullmer, W.D. (2025). *Small-scale validation tests for MFIX-Exa CFD-DEM*; DOE/NETL-2025/4951, NETL Technical Report Series. U.S. Department of Energy, National Energy Technology Laboratory, Morgantown, WV.

An electronic version of this report can be found at:
`https://netl.doe.gov/energy-analysis/search`

Small-scale validation tests for MFIX-Exa CFD-DEM

William D. Fullmer[1]

[1]**National Energy Technology Laboratory, Morgantown, WV 26505**

DOE/NETL-2025/4951

September 24, 2025

NETL Contacts:

Jordan Musser, Principal Investigator

MaryAnn Clarke, Technical Portfolio Lead

Bryan Morreale, Associate Laboratory Director for Research & Innovation

This page intentionally left blank.

Table of Contents

List of Figures

List of Tables

Executive Summary

This report describes several bench-scale fluidization experiments that can be used to validate the CFD-DEM method as encapsulated in the MFIX-Exa code. The five cases considered are the cold-flow fluidized beds of Müller et al. [1, 2], Link et al. [3] (spout-fluid), and Goldschmidt et al. [4] (bi-disperse), the hot fluidized bed of Patil et al. [5, 6], and the adsorbing fluidized bed of Li et al. [7] and Janssen [8]. In most cases, MFIX-Exa with "standard" or "typical" CFD-DEM settings, the Gidaspow drag model, and the Gunn heat transfer provide a relatively good prediction of the quantities considered: mean void fraction profiles, mean velocity profiles, fluctuating velocity profiles, mean particle temperature and segregation index. These results, with other verification and validation tests reported elsewhere, contribute to a body of work providing confidence and credibility in CFD predictions from the MFIX-Exa code.

This report was generated automatically as the output of a regression test using MFIX-Exa version 25.09.

Chapter 1: Introduction

MFIX-Exa (`https://mfix.netl.doe.gov/products/mfix-exa`) is NETL's multiphase computational fluid dynamics (CFD) code for the simulation of particle-laden gas-solid flows. There are two primary modeling options for the solids phase: discrete element method (DEM) or particle-in-cell (PIC). MFIX-Exa was developed for performance and portability by using the AMReX software framework (`https://github.com/AMReX-Codes/amrex`) which provides the iterators, parallel communication routines, and other tools to support highly efficient operations on structured grid and particle data [9, 10]. To date, the code has been scaled out to at least 512 GPUs on ALCF's Aurora and Polaris, NERSC's Perlmutter and OLCF's Frontier and Summit leadership computers.

This work targets "small-scale" particle-laden gas-solid tests (ideally) with experimental data which can be used to "validate" the CFD-DEM method as implemented in the MFIX-Exa code. Small-scale generally refers to bench-scale laboratory experiments. In this case, the scale references the size and time-to-solution of the computational model. Ideally, each case would run on one node in under a day of wall-clock time. As compute power continues to grow; the scale of what can be returned on a days notice also grows. There are air quotes around "validate" because true validation should conclude with a quantitative assessment of model form error [11, 12]. This work stops short of that, presenting qualitative checks of quantitative measurements and leaves it to the user to determine if the quality of the predictive capability presented here is sufficient for their intended use.

This work collects and borrows heavily from previous validation work presented by Fullmer et al. [13], Musser et al. [14], Porcu et al. [15], and Lattanzi et al. [16]. In addition to collecting these works into one place, all of the results presented herein have been refreshed to a recent release of the code: version 25.09. Most importantly, the setup, job submission, and post-processing and creation of this document, has been built into a regression harness so that all cases can be easily re-run with the intent to reproduce this report for every code release. The results will be made available to users via the forum (`https://mfix.netl.doe.gov/forum/c/mfix-exa`). In addition to code updates, slight changes to the model (i.e., inputs) may be observed compared to the previously published results.

Chapter 2: Model

Details of the governing equations can be found in Musser et al. [14] (cold-flow) and Porcu et al. [15] (reacting). Additional details of the DEM model including the linear-spring dashpot model equations can be found in Fullmer et al. [17]. Furthermore, details of the numerical method are not provided here. All of the cases in this report use the Godunov method which is provided by Porcu et al. [15].

What *is* provided here are some of the guiding principles used to set up the benchmark cases. One of the most important parameters is the size of the Eulerian mesh. It is convenient to write the non-dimensional grid spacing as

$$dx^* = \sqrt[3]{dx\ dy\ dz}/d_p. \tag{1}$$

Numerous previous CFD-DEM studies have produced a common heuristic of $1 \leq dx^* \leq 5$, e.g., see [18]. Below a grid size of approximately one (really closer to about 1.2 in my experience), the typical, traditional fluid-to-grid deposition methods start to fail. There are methods to circumvent such issues when $dx^* < 1$ is required, but, at the time of this writing, the diffusion filtering in MFIX-Exa is relatively untested. In a preliminary study on a single realization of a fixed bed, Fullmer and Musser [19] found that the discretization error is small for $dx^* \leq 2$. Where possible, I try to set the fluid mesh $dx^* \approx 2$.

The interfacial mass, momentum, and heat transfer closure models are the most commonly tuned sub-models in multiphase flow CFD. It is common to swap, tune, or significantly modify these sub-models to find the best fit to the data. In this work, I use only the empirical drag model of Gidaspow [20, 21, 22, 23] and the heat transfer coefficient of Gunn [24]. This is an effort to assess the predictive capability of the model "as-is." At a minimum, it will hopefully provide a jumping off point for users applying the code for practical purposes for which data validation does not exist.

Another significant source of uncertainty in (soft-sphere) CFD-DEM simulations is the spring constant of the collision model. In the absence of cohesion [25] or heat transfer [26], particles are typically made as soft

as possible while retaining solution insensitivity. The spring constant is related to the collision time scale by

$$\tau_{coll} = \pi / \sqrt{\frac{k_n}{\hat{m}_{ij}} - \left(\frac{\eta_n}{2\hat{m}_{ij}}\right)^2}, \tag{2}$$

where k_n and η_n are the normal spring constant and dashpot coefficients, respectively, and $\hat{m}_{ij} = m_i m_j/(m_i + m_j)(m_i^{-1} + m_j^{-1})^{-1}$ is the effective mass (twice the harmonic mean) of particle i and particle j. Typically, I assume that the smallest hydrodynamic time-scale of interest is approximately $\mathcal{O}(10^{-3})$ s and set the collision time to $\tau_{coll} \approx 10^{-4}$ s. The general idea is that even soft collisions will seem nearly instantaneous to the fluid if there is at least an order of magnitude separation in time scales. Admittedly, this may be too soft in some instances.

Unless otherwise noted, the simplified tangential spring-dashpot model is applied. Specifically, the history term is neglected leaving only Coulomb friction, see Capecelatro et al. [27] and Fullmer et al. [17]. The tangential spring-dashpot coefficients are typically set following heuristic guidance from Shäfer et al. [28], Silbert et al. [29], Garg et al. [30] and others which suggest $k_t/k_n = 2/7$ and $\eta_t/\eta_n = 1/2$. Here, I follow our own heuristic findings [17] and set $k_t/k_n = 0.9$ and $\eta_t/\eta_n = 0.9$, unless otherwise noted. Additionally, the subcycling is set to 32, i.e., $dt_{DEM} = \tau_{coll}/32$. The CFD timestep, dt, is allowed to float free, limited by the maximum CFL limit of 0.9 (for the Godunov method).

With the application of a fine mesh ($dx* \approx 2$) and a small DEM timestep ($dt_{DEM} \approx 3.125 \times 10^{-6}$ s), I assume that the largest source of numerical error is statistical, i.e., due to finite time-averaged statistics. The simple method of non-overlapping batch means (NOBM) with a Student t-test coefficient is used to compute 95% confidence intervals (CIs) on the time-averaged data [31]. Time-dependent data would benefit from replicate simulations, but that is not currently considered in these tests.

Currently, MFIX-Exa requires that the mesh spacing be identical in each coordinate direction, $dx = dy = dz$. Usually, this means that any given rectangular fluidized bed will not be discretized by an integer number of fluid cells in both transverse dimensions. Discrepancies are typically handled by setting one dimension to an integer value and off-setting the other dimension within the domain so that cells are equally cut on either side of the center-plane to preserve symmetry. The streamwise dimension of the bed is frequently extended from the experimental (physical) value to a "nice" value, i.e., an integer number of fluid *grids* (the unit for MPI work). It is assumed that this does not affect the flow dynamics in the lower region of interest.

Chapter 3: Müller cold-flow fluidized bed

The first case considered here is probably *the* quintessential CFD-DEM validation test. The experiment of Müller et al. [1, 2] consisted of a bench-scale, "pseudo-2-D,"[1] clear bed of poppy seeds fluidized by air. Due to the moisture in the seeds, high-speed spatio-temporal MRI measurements of solids concentration and velocity were collected. It should be noted that several fundamental assumptions of the CFD-DEM model are stressed in this case due to the irregularity of the particles which are non-spherical with significant surface irregularity. The seeds were measured to have a minimum fluidization velocity of $U_{mf} = 0.3$ m/s. The bed was fluidized from below by a uniform distributor at $U_{in} = 3U_{mf}$. In the first paper [1], particle velocity was measured with a spatial resolution of 0.94×0.94 mm^2 resulting in 47 locations spanning the bed width. Mean particle vertical velocity was reported at three elevations: $y = 15$, 25 and 35 mm above the distributor. Mean gas-phase volume fraction profiles were reported in the second paper [2] at two elevations: $y = 16.4$ and 31.2 mm. Additionally, the bed was operated at (and data reported for) a lower superficial velocity, $U_{in} = 2U_{mf}$. For volume fraction, the MRI resolution was roughly twice as large, 1.9×2.2 mm^2. It is assumed that the first coordinate corresponds to x as there are 22 data points spread across the width of the bed.

The Müller experiment is simulated in MFIX-Exa using the incompressible gas constraint with a constant density. Details of the simulation parameters are provided in Table 1. A fluid mesh of $N_x \times N_y \times N_z = 32 \times 128 \times 8$ is applied. Note that this fluid mesh gives a dimensionless resolution of $dx^* \approx 1.15$ which is

[1] It is common for bench-scale experiments of granular and particle-laden flows to be thin in one dimension to permit optical access. Such experiments are often referred to as pseudo-two-dimensional. However, true two-dimensional flows would have no wall effects in the thin dimension. Conversely, thin experiments have extreme wall effects in the thin dimension. This can be challenging for the CFD-DEM method which, typically, does not resolve the gas-phase wall boundary layer.

Table 1: Summary of experimental properties and simulation parameters of the Müller fluidized bed.

property	symbol	value	units
bed width	L_x	44	mm
bed height	L_y	176	mm
bed depth	L_z	10	mm
grid size	dx^*	1.15	
particle count	N_p	9240†	
particle diameter	d_p	1.2	mm
particle density	ρ_p	1000	kg/m^3
p-p restitution coefficient	e_{pp}	0.95	
p-w restitution coefficient	e_{pw}	0.95	
p-p friction coefficient	μ_{pp}	0.1	
p-w friction coefficient	μ_{pw}	0.1	
spring stiffness	k_n	440	N/m
collision duration	τ_{coll}	1×10^{-4}	s
fluid density	ρ_g	1.2	kg/m^3
fluid viscosity	μ_g	1.8×10^{-5}	Pa-s
inlet superficial velocity	U_{in}	0.6, 0.9	m/s

†See text for further comment.

roughly half of the target resolution. This higher resolution is applied here because, otherwise, there would only be two uncut fluid cells in the depth of the bed. The bed is defined by an EB `box` that fills domain in x and is centered in z. The edge cells in the depth of the bed are approximately one-third covered. A uniform mass inflow is set at $y = 0$ and a constant pressure outflow at the top $y = L_y$. The inflow velocity is ramped up in time from $U_{in} = 0.4$ m/s at time zero to 0.6 m/s at $t = 1$ s and 0.9 m/s at $t = 2$ s (for the $3U_{mf}$ case). The Gidaspow drag model is applied. The actual minimum fluidization velocity was not determined for this setup, so it is unknown exactly what these flow rates are relative to the simulation U_{mf}. The particles are initialized one-per-cell up to an elevation of $y = 67.375$ mm ($49dx$) giving 9144 total particles, approximately 100 fewer than reported in the experiment.

Monitors are used to calculate volume fraction and velocity profiles. Each individual monitor is taken to be $2dx$ in width, $2dx$ in height, and spanning the full bed depth. The elevation corresponds to the nearest fluid mesh edge to the experimental value. For velocity profiles, this is: $y = 15.125$ ($11dx$), 24.75 ($18dx$), and 34.375 mm ($25dx$) and for volume fraction profiles this is: $y = 16.5$ ($12dx$) and 31.625 mm ($23dx$). Therefore, neither the elevations nor the size of the averaging regions exactly match the experiment. Monitor data of both types is collected at a frequency of 100 Hz. Currently, there are no checks in place to ensure there are particles in each velocity monitor region. Initial testing has showed that it is relatively rare for monitors to be completely devoid of particles, but there are likely a few zeros averaged into the means that should be neglected.

Simulations are run for a time of 55 s. The first 5 s of data is discarded as initial start up transient and the 50 s is split into ten non-overlapping batch means of $\delta t = 5$ s intervals. The mean of the means is reported with error bars corresponding to 95% confidence intervals determined from a t-test. The results are compared to the experimental data in Figures 1 and 2. The volume fraction profiles match relatively well at the lower elevation but are much more flat compared to the data at the upper elevation. This result is consistent with previous CFD-DEM validation tests including the original MFiX code [32] and Müller et al. [2]. The velocity profiles are also quite similar to previously published results [1, 32] showing a general over-prediction, agreement, and under-prediction of peak centerline particle velocity moving up the three measurement elevations. As an interesting aside, velocity data at the lower elevation is accurately predicted by particle-resolved direct numerical simulation (PR-DNS) [33], suggesting that the discrepancy *could* be inherent to the unresolved CFD-DEM approach. Similarly, the present results fail to capture the sharp up-turn in the higher elevation profiles close to the walls. Again, this is consistent with other previous CFD-DEM studies [1, 32] but is more accurately captured with PR-DNS [34].

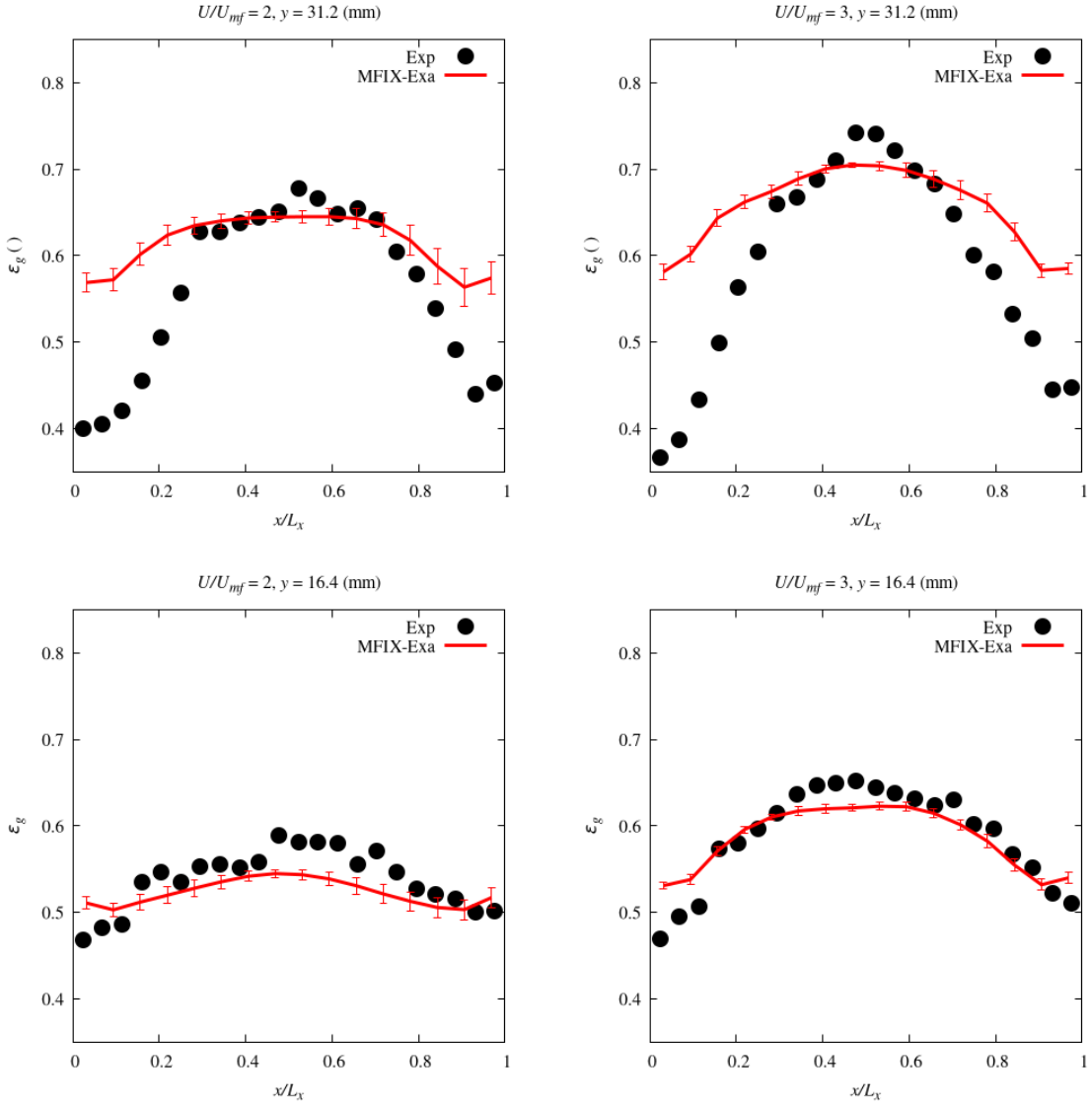

Figure 1: Comparison of width-spanning gas volume fraction profiles between MFIX-Exa simulation and the experiment of Müller et al. [1, 2].

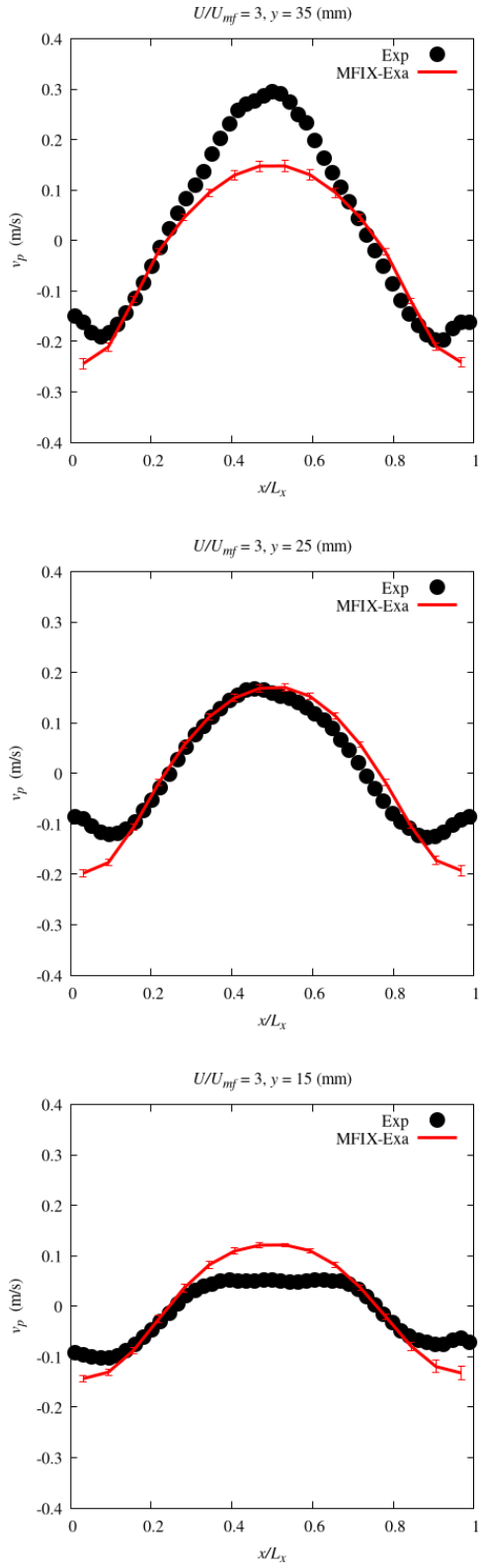

Figure 2: Comparison of width-spanning particle vertical velocity profiles between MFIX-Exa simulation and the experiment of Müller et al. [1, 2].

Chapter 4: Link cold-flow spout-fluidized bed

The experiment of Link et al. [3] was a bench-scale spout-fluidized bed. Unlike many other bench-scale fluidized beds, the Link bed is not "pseudo-2-D," with a bed depth $L_z = 84$ mm over half the width $L_x = 154\ mm$. Additionally, this case is not uniformly fluidized. Instead, a 22 mm wide and 12 mm deep high velocity jet is centered on the inlet plane. The jet is surrounded by a lower velocity gas distributor for uniform fluidization of the bulk. The dual-inlet bed allows the sweeping of a 2-D flow-regime map between spouted bed and fluidized bed behavior [3]. Experimental data was collected from three conditions:

- case B1: $U_{in} = 2.5$ m/s, $U_{jet} = 60$ m/s, flow regime: intermediate spout-fluidization
- case B2: $U_{in} = 2.5$ m/s, $U_{jet} = 90$ m/s, flow regime: spouting with aeration
- case B3: $U_{in} = 3.5$ m/s, $U_{jet} = 65$ m/s, flow regime: jet in fluidized bed

Data on particle velocity was collected by means of positron emission particle tracking (PEPT). Mean and fluctuating (standard deviation) vertical velocity profiles were reported at elevations of $y = 15$ and 25 mm. Horizontal fluctuating velocity profiles were also reported but are not utilized in this work. The spatial averaging region for this data is the central z-plane that spans the same depth as the jet inlet. The profiles were given in 14 points for a resolution of $\delta x = 11$ mm. By counting the number of points in a quiver plot, it appears that the vertical resolution, i.e., height of the regions used to calculate the profile data, is approximately $\delta y = 10$ mm. The particle properties needed for CFD-DEM simulation were measured and reported, see Table 2.

Table 2: Summary of experimental properties and simulation parameters of the Link spout-fluidized bed.

property	symbol	value	units
bed width	L_x	154	mm
bed height	L_y	1000†	mm
bed depth	L_z	84	mm
grid size	dx^*	2.97	
particle count	N_p	44800†	
particle diameter	d_p	4.04	mm
particle density	ρ_p	2526	kg/m^3
p-p restitution coefficient	e_{pp}	0.97	
p-w restitution coefficient	e_{pw}	0.97	
p-p friction coefficient	μ_{pp}	0.1	
p-w friction coefficient	μ_{pw}	0.1	
spring stiffness	k_n	4.3×10^4	N/m
collision duration	τ_{coll}	1×10^{-4}	s
fluid density	ρ_g	1.2	kg/m^3
fluid viscosity	μ_g	1.8×10^{-5}	Pa-s
inlet superficial velocity	U_g	†	m/s

†See text for further comment.

The experiment is simulated in MFIX-Exa using the incompressible gas constraint with a constant density. Details of the simulation parameters are provided in Table 2. The fluid cell size is $dx = 12$ mm, $dx^* \approx 3$, with a fluid mesh of $32 \times 128 \times 8$, yielding a slightly larger domain in all three dimensions than the experimental bed. The bed is defined by an EB `box` which is centered in z but placed flush with $x = 0$ so that a full integer number of cells are applied across the depth. The location of the `box` within the domain is sketched in Figure 3. The bed is allowed to simply be 56 mm taller than in the experiment. The jet region is modeled as covering two fluid cells. Hence, the width of the jet, 24 mm, is wider than in the experiment, 22 mm, while the depth, 12 mm, is consistent. This area difference is non-negligible, approximately 9% larger. Therefore, the jet velocity is adjusted from the reported values of $U_{jet} = 60$, 90, and 65 m/s down to $U_{jet} = 55$, 82.5,

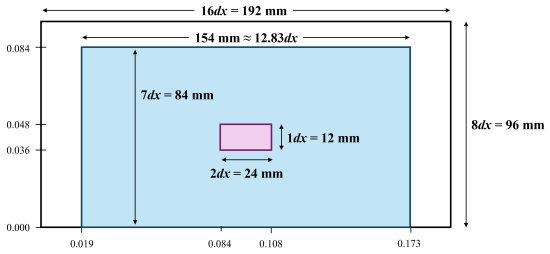

Figure 3: Sketch of the domain, geometry, and boundary conditions of the MFIX-Exa simulations in the x-z plane.

and 59.58 m/s to preserve the volumetric flux. The area of uniform inlet region is correspondingly smaller as well. However, this area difference, approximately 0.2% smaller, is negligible and U_{in} is not adjusted. The boundary velocities U_{in} and U_{jet} are constant in time, i.e., no ramping up. A constant pressure outflow is set at the top $y = L_y$. The Gidaspow drag model is applied. Particles are initialized eight-per-cell up to an elevation of $y = 816$ mm ($68dx$) giving $N_p = 45076$ total particles, 276 more than reported in the experiment.

Monitors are used to calculate velocity profiles. Because we are only interested in Lagrangian data in this case, the monitors are set independent of the fluid mesh and are of size $\delta x = 11$ mm, $\delta_y = 10$ mm and $\delta z = 12$ mm and centered on the jet region and at elevations of $y = 15$ and $y = 25$ mm as in the experiment. The time scale of hydrodynamics in this spout-fluidized bed is smaller than the other uniformly fluidized beds. It is found that $\delta t = 2$ s bins are sufficient for time-averaging the velocity profiles. Ten non-overlapping bins are used to collect temporal statistics beginning after a 2 s start-up period. Monitors data is collected at a frequency of 200 Hz. Currently, there are no checks in place to ensure there are particles in each velocity monitor region. Initial testing has showed that it is rare for monitors to be completely devoid of particles outside of the start up period.

The velocity profiles for all three flow conditions are shown in Figures 4 - 6. Mean velocity profiles are generally in good agreement with the data. The largest discrepancy appears at the lower elevation of case B2 where the simulation predicts a much stronger recirculating spout flow than observed in the experiment and previous CFD-DEM solutions [3, 32]. This could be due to the wider jet inlet region or possibly the neglect of tangential friction in the collision model. The fluctuating particle velocity profiles show acceptable agreement with the data. It should be noted that there is a fundamental difference in the data reported from the simulations and in the experiments which may be exacerbated for fluctuating velocity. In the experiments, a single particle is radioactively tagged and tracked with PEPT. Therefore, each individual piece of data comes from a single particle which is averaged over recurrence through a given region. In the simulation, all particles within a given region (i.e. monitor) are averaged and this average particle velocity at a given time is taken as the individual piece of data and time-averaged to determine mean and fluctuating velocities.

Chapter 5: Goldschmidt cold-flow bi-disperse fluidized bed

The experiment of Goldschmidt et al. [4] was another small-scale "pseudo-2-D" fluidized bed uniformly fluidized from below. In this case, however, the particles were a bi-dispersed (size) mixture of large, 2.5 mm, and small, 1.5 mm, diameter glass beads. The bed and material properties are summarized in Table 3. The original experiments considered a wide range of conditions varying static bed height, the mass fraction, and inflow velocities. Data was collected by digital image analysis of the mean heights of the two particle types to determine segregation behavior. The segregation index, s is defined as

$$s = \frac{S - 1}{S_{\max} - 1} \ , \tag{3}$$

where $S = \overline{y_1}/\overline{y_2}$ is the ratio of the mean elevation of the small-to-large particles and

$$S_{\max} = \frac{2 - X_1}{1 - X_1} \ , \tag{4}$$

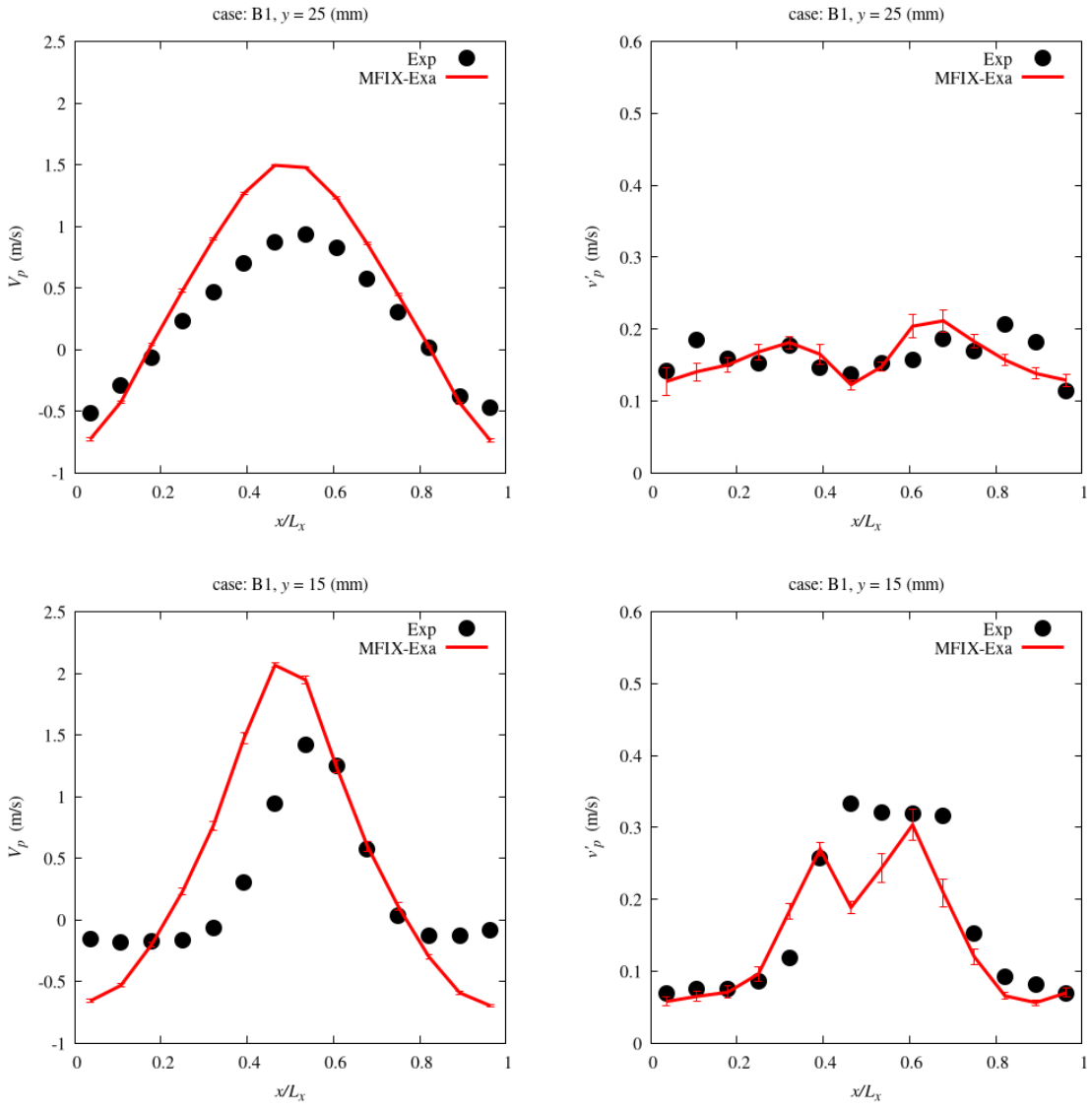

Figure 4: Comparison of width-spanning mean (left) and fluctuating (right) streamwise particle velocity profiles between MFIX-Exa simulation and the experiment B1 of Link et al. [3].

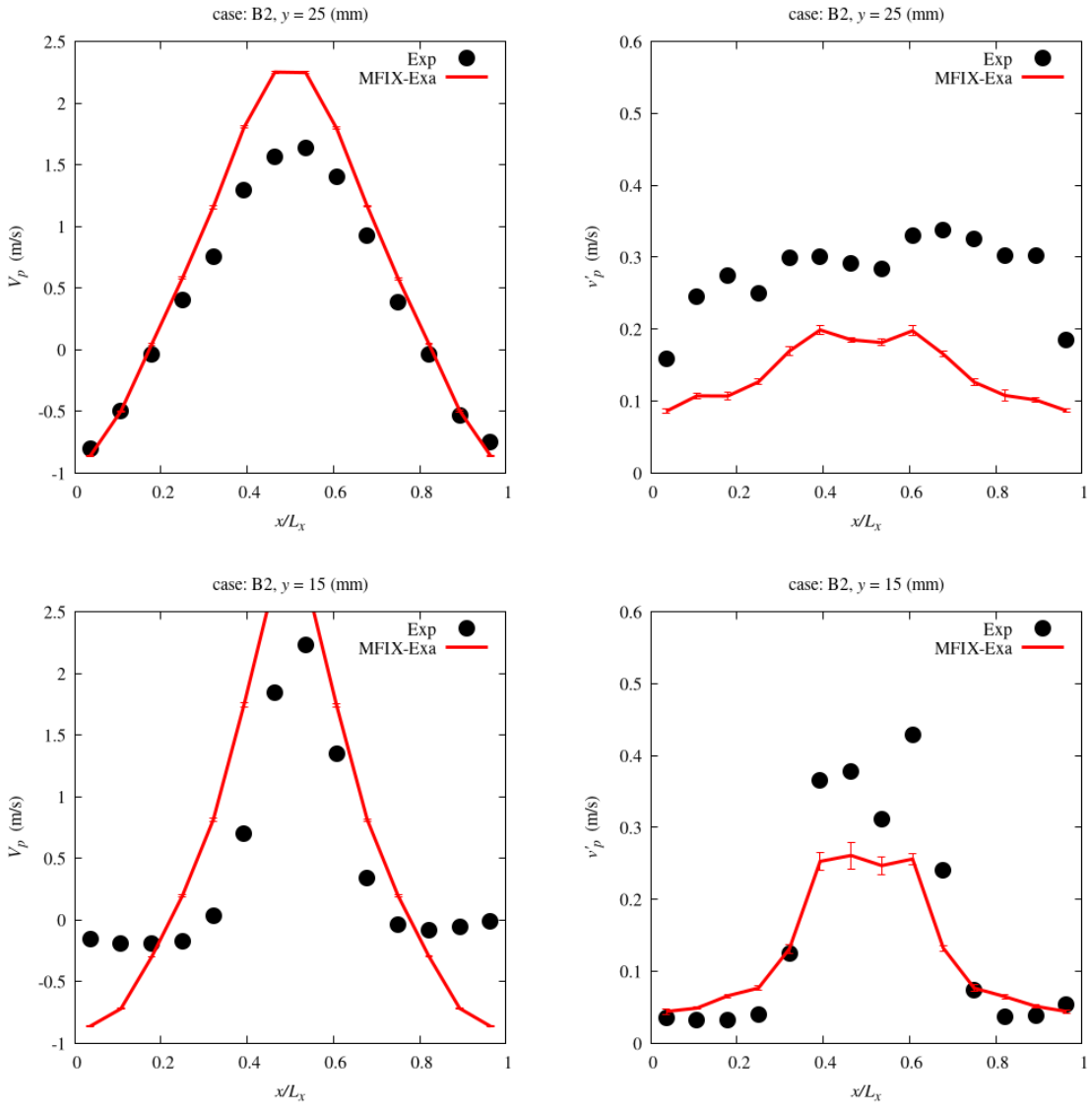

Figure 5: Comparison of width-spanning mean (left) and fluctuating (right) streamwise particle velocity profiles between MFIX-Exa simulation and the experiment B2 of Link et al. [3].

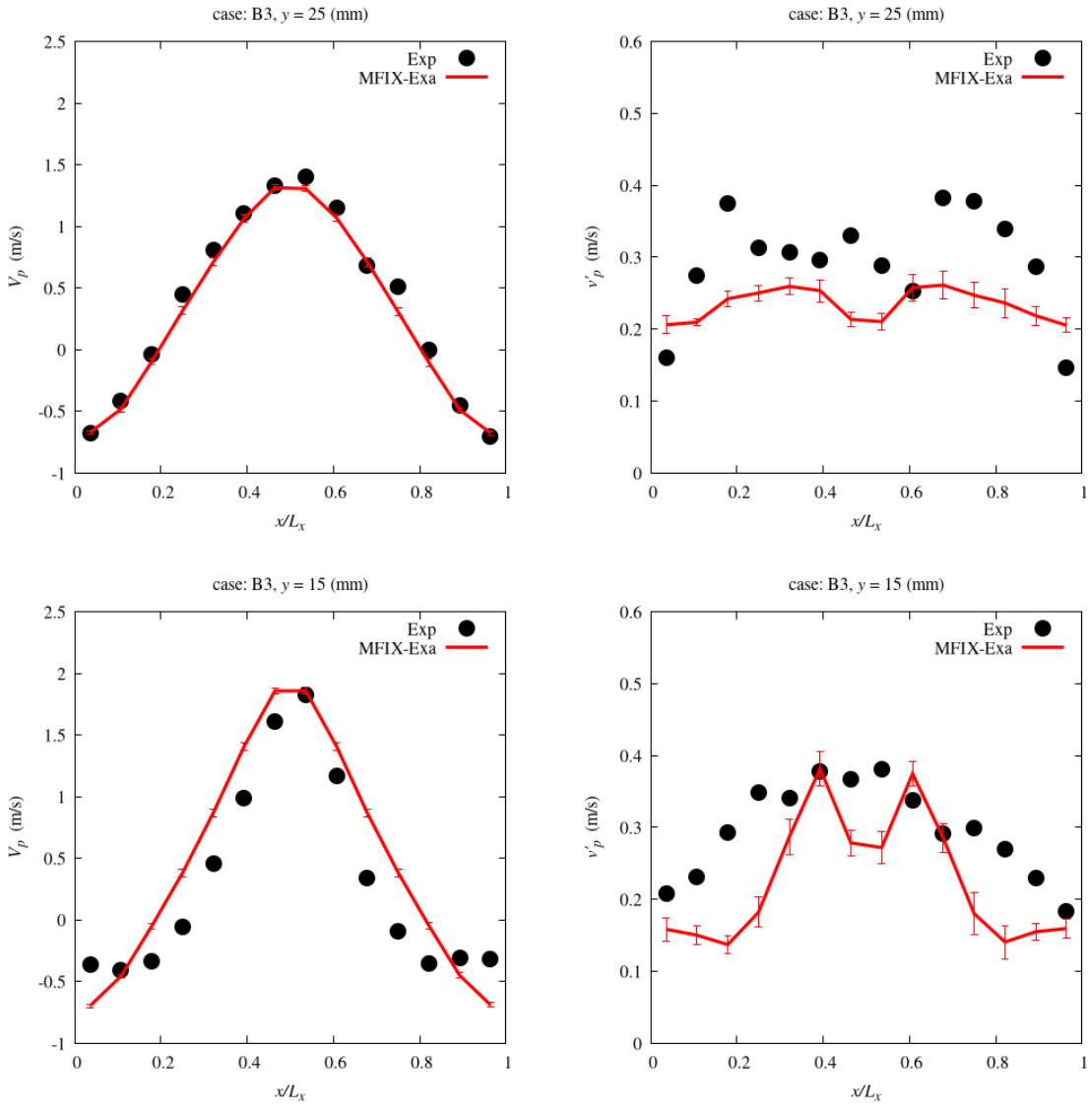

Figure 6: Comparison of width-spanning mean (left) and fluctuating (right) streamwise particle velocity profiles between MFIX-Exa simulation and the experiment B3 of Link et al. [3].

Table 3: Properties of the Goldschmidt fluidized bed as reported [4]. Several adjustments have been made for modeling purposes, please refer to the text.

property	symbol	value	units
bed width	L_x	150	mm
bed height	L_y	700	mm
bed depth	L_z	15	mm
static bed height	h	150	mm
grid size	dx^*	2.5, 1.5	
small particle diameter	d_1	1.51 ± 0.04	mm
large particle diameter	d_2	2.49 ± 0.02	mm
small particle density	ρ_1	2523 ± 6	kg/m^3
large particle density	ρ_2	2526 ± 6	kg/m^3
p-p restitution coefficient	e_{pp}	0.97 ± 0.01	
1-1 friction coefficient	μ_{11}	0.15 ± 0.015	
2-2 friction coefficient	μ_{22}	0.10 ± 0.01	
1-w friction coefficient	μ_{1w}	0.10 ± 0.01	
2-w friction coefficient	μ_{2w}	0.09 ± 0.01	
spring stiffness	k_n	2290.3	N/m
collision duration	τ_{coll}	1×10^{-4}	s
fluid density	ρ_g	1.2	kg/m^3
fluid viscosity	μ_g	1.8×10^{-5}	Pa-s
inlet superficial velocity	U_g	1.15	m/s

is the theoretical maximum degree of segregation and X_1 is the mass fraction of small particles.

Some adjustments and simplifications have been made in the MFIX-Exa model of the Goldschmidt experiment. The actual height of the test section was extended to be an integer number of the bed width, $L_y = 750$ mm. The bed is resolved by a uniform $dx = 3.75$ mm fluid mesh with an EB `box` placed just inside the domain extents, `offset = 1e-9`. The measured density of the two particles differed slightly in mean value but had overlapping error bars. Here, the particles are treated as a single solids type of density $\rho_p = 2525$ kg/m^3. Further, single particle-particle, $\mu_{pp} = 0.15$, and particle-wall, $\mu_{pw} = 0.1$, friction coefficients are applied. The spring constant is set such that the collision time of a small-small particle collision is $\tau_{coll} = 1 \times 10^{-4}$ s. This gives small-large and large-large particle collision times of $\tau_{coll} = 1.3 \times 10^{-4}$ s and $\tau_{coll} = 2.1 \times 10^{-4}$ s, respectively.

Although many conditions are considered in the original work [4], the focus here is restricted to two mass fractions at a single inlet superficial gas velocity of $U_g = 1.15$ m/s and static bed height of $h = 15$ cm. When the small particle solids mass fractions is $X_1 = 0.25$ the mixture readily segregates and when the small particle solids mass fractions is $X_1 = 0.75$ the mixture does not segregate. This provides a simple yes/no test of the model.

The experiment is simulated in MFIX-Exa using the incompressible gas constraint with a constant density. Because the particles are not very different, size ratio $d_2/d_1 \approx 5/3$, the Gidaspow drag model is used without any polydisperse corrections [35]. The static bed height is assumed to have a solids volume fraction near monodisperse maximum packing, $\phi_0 = 0.64$. Then, the number of small particles can be computed from

$$N_1 = \frac{6 X_1 \phi_0 L_x h L_z}{\pi d_1^3} \ . \tag{5}$$

For small particle mass fractions of $X_1 = 0.25$ and 0.75, Eq. (5) gives $N_1 = 29400$ and 881000, respectively. The number of large particles is then set by

$$N_2 = N_1 \frac{X_2}{X_1} \left(\frac{d_1}{d_2} \right)^3 \ , \tag{6}$$

giving $N_2 = 20000$ and 6700 for the same conditions. Particles are seeded randomly in the entire domain using a custom particle generation script, placing all large particles first.

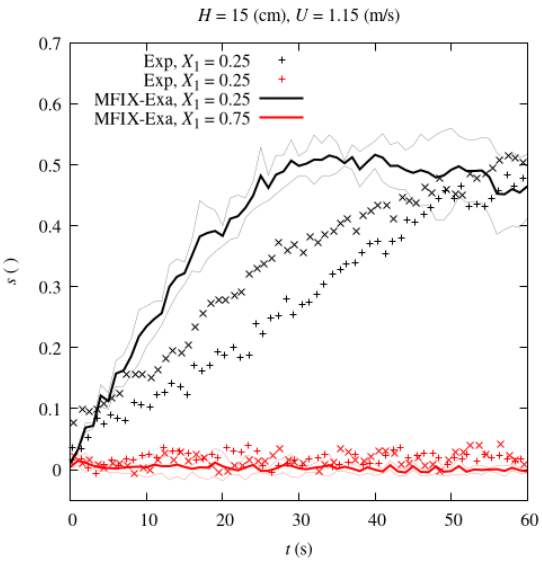

Figure 7: Comparison of the segregation index between MFIX-Exa simulation and the experiment of Goldschmidt et al. [4]. Note that both replicates of each experiment are provided.

The inflow velocity is set at $U_{in} = 0.8$ m/s for a period of $t = 1.8$ s. This velocity should be below the small particle minimum fluidization velocity and allow the mixture to settle into a random, uniform, packed bed. Between $t = 1.8$ and 2.0 s, the velocity is abruptly ramped up to the experimental condition value and simulated for an additional 60 s, and the first 2 s of simulation time is disregarded. Each condition is simulated five times, each replicate using a different seed in the random number generator used to generate the initial particle arrays, thereby creating a statistically unique condition.

Monitors are not used for this benchmark problem. Rather, native AMReX plot files are saved at a frequency of 1 Hz and a python script leveraging the yt visualization package is used to compute the mean heights, $\overline{y_1}$ and $\overline{y_2}$, and the segregation index, see Eq. (3). The mean and the 95%-confidence interval of the five replicates is reported at each time and shown in Figure 7 against the experimental data. The expected results are observed: with the small particle mass fraction is low, $X_1 = 0.25$, strong segregation is observed, but when the small particle mass fraction is high, $X_1 = 0.75$, essentially no segregation takes place. In this case, the mass fraction dependence occurs because the inlet velocity is between the minimum fluidization velocities of the two material. When the small particles are relatively few, they percolate out and form a fluidized layer above a relatively de-fluidized layer. Conversely, when there are many small particles the entire bed remains fluidized providing good mixing for the large particles. The the $X_1 = 0.25$ case, the predicted segregation rate is higher/faster than the experimental data. This is in-line with previous studies [36, 32] that have found improved prediction by using a polydispere correction factor [35], which is currently not implemented in MFIX-Exa.

Chapter 6: Patil thermal fluidized bed

The experiment of Patil et al. [5, 6] is a bench-scale, "pseudo-2-D" fluidized bed. Unlike previous validation tests in this report so far, the Patil bed is a heat transfer problem. The particles, glass beads, are heated in an oven then dropped into the bed and fluidized by a cool gas. Both references [5] and [6] state that the particles were heated to a temperature of 120 °C (393.15 K), however the provided data indicate an initial temperature of approximately 90 °C (363.15 K). It is unknown if the 30 °C discrepancy was simply an error or if the particles cooled during the transition from the oven to the start of fluidization. The bed was `almost` uniformly fluidized from below by a perforated plate distributor "background" velocities of $u_{bg} = 1.20$, 1.54, 1.71 (m/s). These velocity values assume a uniform inlet, i.e., an inlet cross-sectional area of $A_{bg} = L_x \times L_z$. However, there was also a jet inlet region of diameter $D_j = 13$ mm centered in the bottom

of the bed. Similar to the Link experiment [3], the jet could be used for spouted or spout-fluidized operation, though it was inactive in these experiments [5, 6]. The initially hot particles were cooled by the fluidizing gas (nitrogen) which was measured and recorded with an infrared (IR) camera. The primary quantity of interest is therefore the mean global solids temperature as a function of time. There was also temperature data collected for smaller 0.5 mm glass beads, but the coverage is not as comprehensive and only the 1 mm particles are considered here. A "standard," visual camera was simultaneously used to collect image pairs and processed with particle image velocimetry (PIV) and reported as solids mass flux profiles, though unused in this work. Finally, we will note that the minimum fluidization velocity of the particles was reported to be $U_{mf} = 0.58$ m/s.

Table 4: Summary of experimental properties and simulation parameters of the Patil bed.

property	symbol	value	units
bed width	L_x	80	mm
bed height	L_y	250†	mm
bed depth	L_z	15	mm
grid size	dx^*	2	
wall temperature	T_w	293.15	K
bed mass	M	75, 125†	g
particle diameter	d_p	1.0	mm
particle density	ρ_p	2500	kg/m^3
initial particle temperature	$T_{p,0}$	363.15	K
particle heat capacity	$c_{p,p}$	840	J/kg-K
p-p restitution coefficient	e_{pp}	0.97	
p-w restitution coefficient	e_{pw}	0.97	
p-p friction coefficient	μ_{pp}	0.33	
p-w friction coefficient	μ_{pw}	0.33	
spring stiffness	k_n	646	N/m
collision duration	τ_{coll}	1×10^{-4}	s
fluid molecular weight	W_g	0.028013	kg/mol
fluid viscosity	μ_g	1.75×10^{-5}	Pa-s
fluid heat capacity	$c_{p,g}$	1041‡	J/kg-K
fluid thermal conductivity	κ_g	0.0254	W/m-K
fluid inlet superficial velocity	U_{in}	$1 \sim 2^\dagger$	m/s
fluid inlet temperature	T_{in}	293.15	K

†See text for further comment.

‡Patil et al. [6, 5] gave a value of $c_{p,g} = 1010$ J/kg-K.

The Patil experiment is simulated in MFIX-Exa using the ideal gas (open system) constraint, advecting both density and enthalpy. Transport equations for species are not considered because the only species are nitrogen gas and solid glass. Details of the experiment are summarized in Table 4. The fluid cell size is $dx = 2$ mm, $dx^* = 2$, with a fluid mesh of $40 \times 128 \times 8$, yielding a slightly taller and deeper domain than the bed. The bed is defined by an EB `box` which is centered in z. Therefore, the first and last cells in the z-direction are 25% covered. The extra height is not corrected. A pressure outlet is placed at the top set to atmospheric conditions, $p_{out} = 101325$ Pa. A uniform inflow is placed at the bottom of the bed. The inactive jet is also modeled as a mass inflow of zero velocity. Although the actual jet was circular, it is modeled as a rectangular region centered at the inlet plane of size $8dx \times 4dx$, approximately 45% larger than the actual jet area. This adjustment was made so that there is at least one full cell between the edge of the jet region and the front and back walls. The active area of the inlet is then $A_{in} = L_x L_z - 32dx^2$, which is only approximately 4% smaller than the actual active area in the experiment. The inlet velocities, $U_{in} = U_{bg} L_x L_z / A_{in} = 1.343$, 1.724, and 1.914 m/s, are constant in time, i.e., no ramping up. The Gidaspow drag model and the Gunn heat transfer coefficient model are applied. Particles are initialized eight-per-cell up to an elevation of $y = 54$ mm ($27dx$) for the $M = 75$ g case and $y = 88$ mm $= (44dx)$ for the $M = 125$ g

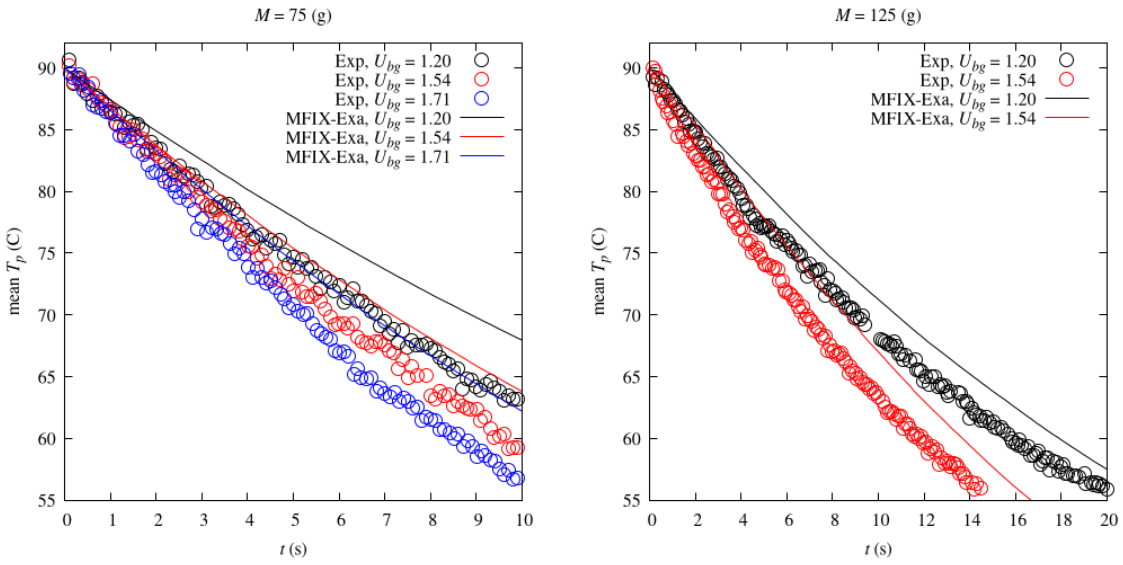

Figure 8: Comparison of mean particle temperature between MFIX-Exa simulation and the experiment Patil et al. [5, 6].

case. The actual number of seeded particles for these two cases are $N_p = 57876$ and 95004 for total bed masses of 75.76 g and 124.36 g, respectively. Note that the larger bed mass did not operate at the highest inlet velocity. The initial particle temperature is $T_{p,0} = 363.15$ K and the gas-phase initial temperature $T_{g,0}$, inlet temperature T_{in}, and the wall boundary temperature T_w are all set to 293.15 K.

A single monitor is used to calculate the (Lagrangian-) mean particle temperature. The cooling curves predicted by MFIX-Exa are compared to the experimental data in Fig. 8. Generally, there is acceptable agreement overall. The predicted cooling rate is lower/slower, resulting in a higher mean particle temperature in all cases. The difference is larger for smaller 75 g bed. Some of the missing heat loss is possibly due to the constant bed wall temperature assumption.

Chapter 7: Li-Janssen adsorbing fluidized bed

The experiment of Li et al. [7] and Janssen [8] (collectively referred to as Li-Janssen) is a bench-scale, "pseudo-2-D" fluidized bed. The bed had the same dimensions as that used in the Patil et al. [5, 6], including the non-uniform wall materials.[2] Physically, the experiment extended from a heat transfer problem of the Patil experiment to include an adsorption "reaction." In this case, the adsorbent was 1.9 mm diameter zeolite 13X particles and the absorbate was CO_2 delivered in the fluidizing gas, a mixture of N_2 and CO_2. Note that this is physisorption not chemisorption, i.e., the electron structure of bonding molecules is not changed. This adsorption process is exothermic, releasing heat as CO_2 is bound to the clean, regenerated zeolite particles. Hence, the mean particle temperature was the primary quantity of interest captured in the experiments through the same IR camera and image processing techniques as in Patil et al. [5, 6].

The Li-Janssen experiment is simulated in MFIX-Exa using the ideal gas (open system) constraint, advecting density, enthalpy, and species. The Gidaspow drag model and the Gunn heat transfer coefficient model are applied. Details of the experiment are summarized in Table 5. Because the particle diameter is roughly twice as large as in the Patil experiment, so too is the fluid cell size: $dx = 4$ mm, $dx^* = 2.1$, a fluid mesh of $24 \times 64 \times 4$. The bed is defined by an EB `box` centered in the x-z plane. Note that, in the z-direction, the bed is resolved by only two full and two cut cells. The extra height is not corrected. A pressure outlet is placed at the top, $p_{out} = 98320$ Pa. A uniform inflow is placed at the bottom of the bed setting $U_{in} = 1.2$ m/s and $T_{in} = 289.15$ K, which is constant in time. However, the constituent species, N_2

[2]Although every indication is that the Li-Janssen experiment and the Patil experiment used the same bed, I found no discussion in Li et al. [7] or Janssen [8] about the non-uniform inlet. Therefore, a single uniform inlet boundary condition is applied in this case.

Table 5: Summary of experimental properties and simulation parameters of the Patil bed.

property	symbol	value	units
bed width	L_x	80	mm
bed height	L_y	250†	mm
bed depth	L_z	15	mm
grid size	dx^*	2.1	
wall temperature	T_w	302.5‡	K
bed mass	M	40†	g
particle diameter	d_p	1.9	mm
particle density	$\rho_{p,0}$	1100	kg/m^3
initial particle temperature	$T_{p,0}$	297	K
particle heat capacity	$c_{p,p}$	760	J/kg-K
p-p restitution coefficient	e_{pp}	0.95	
p-w restitution coefficient	e_{pw}	0.95	
p-p friction coefficient	μ_{pp}	0.4	
p-w friction coefficient	μ_{pw}	0.2	
spring stiffness	k_n	1950	N/m
collision duration	τ_{coll}	1×10^{-4}	s
fluid viscosity	μ_g	1.782×10^{-5}	Pa-s
fluid heat capacity	$c_{p,g}$	mixture†	J/kg-K
fluid thermal conductivity	κ_g	0.0259	W/m-K
fluid inlet superficial velocity	U_{in}	1.2	m/s
fluid inlet temperature	T_{in}	289.15	K
fluid inlet CO_2 mole fraction	Y_{g,CO_2}	20, 40, 60	%

†See text for further comment.

‡Janssen [8] gives the value of 302.5 K which is used in the MFIX-Exa model; Li et al. [7] gave and used a value of 300 K.

and CO_2, are ramped down/up in time. Three conditions are considered with CO_2 volume or mole fractions of $Y_{g,CO_2} = 0.2$, 0.4, and 0.6, with N_2 to balance in all cases. The molecular weight of N_2 and CO_2 are $W_{g,N_2} = 0.028013$ kg/mol and $W_{g,CO_2} = 0.04401$ kg/mol, respectively. Therefore the inlet gas mass mass fractions of CO_2 are $X_{g,CO_2} = 0.282$, 0.5116, and 0.7021, again with N_2 to balance, for the three conditions. The species diffusivity coefficient is $\mathcal{D}_g = 16 \times 10^{-6}$ m^2/s.

The initial bed mass of regenerated (clean) zeolite was reported to be $M = 40$ g. Particles are initialized eight-per-cell up to an elevation of $y = 92$ mm ($23dx$) resulting in $N_p = 10508$ particles and an initial bed mass of $M \approx 41.5$ g. The initial particle temperature is a bit of an unknown. In Li et al. [7], Table 1 indicates that the initial particle temperature in the CFD-DEM simulations was likely $T_{p,0} = 296.5$ K, while Fig. 5 indicates that $T_{p,0}$ may have been a little under 295 K in the experiments. Here, the time-zero particle temperature is set to $T_{p,0} = 297$ K. However, the particles cool as they are fluidized by the gas (at 289.15 K), reaching a mean temperature of approximately 295.5 K at time $t = 3.75$ s when the CO_2 is introduced. The ramp up/down in CO_2/N_2 is linear over a duration of 0.5 s for all inlet concentrations. The time $t = 4$ s is taken as the initial state.

The adsorption process is modeled as a single chemical reaction,

$$CO_2 \rightarrow CO_2(s) \ ,$$

where $CO_2(s)$ refers to gaseous CO_2 that is bound to the zeolite. Therefore, the solid is composed of two species, zeolite and $CO_2(s)$. The bound carbon dioxide is given the same specific heat capacity as the zeolite so that this property does not change with CO_2 loading. The reverse desorption is not modeled. Li [7] and Janssen [8] propose a fractional-order reaction model,

$$\frac{dq}{dt} = k \left(q_e - q\right)^n \ , \tag{7}$$

where q is the CO_2 mass loading, q_e is the equilibrium loading, k is the reaction rate, and n is the fractional-order. The mass loading is given by m/m_0 in (kg/kg) where m is the particle mass at any given time and m_0 is the reduced particle mass, i.e., $m_0 = \rho_{\text{zeolite}}(\pi/6)d_p^3$ when $X_{p,\text{CO}_2(s)} = 0$. Because there are only two species in the particle, the mass loading can be written as $q = X_{p,\text{CO}_2(s)}/X_{p,\text{zeolite}}$. An Arrhenius equation is used for the reaction rate,

$$k = k_0 e^{-E_a/RT} \,, \tag{8}$$

where k_0 is a pre-exponent coefficient, E_a is the activation energy, T is a temperature, and $R = 8.3145$ J/mol-K is the universal gas constant. Although likely very similar, it is unclear if this temperature should be the particle temperature or the gas temperature; the former is assumed here. The activation energy is taken from the work of Dantas et al. [37], $E_a = -29.38$ kJ/mol. The remaining parameters were determined by fitting thermogravimetric analysis (TGA) [8, 7]: $k_0 = 1.5 \times 10^{-5}$ s^{-}1, $n = 2.47$, and q_e as given in Table 6. Finally, the heat of adsorption, ΔH, was measured to be -29.6, -30.2, and -32.1 kJ/mol at temperatures of 30, 50, and 100 °C by a Simultaneous Thermal Analyzer [8]. Here, a constant value is used, $\Delta H = -30$ kJ/mol or -6.82×10^5 J/kg.

Table 6: Equilibrium adsorption, q_e, of CO_2 onto $d_p = 1.9$ mm zeolite 13X particles as a function of CO_2 mole fraction, Y_{g,CO_2}, in a N_2-CO_2 mixture at atmospheric pressure [8].

Y_{g,CO_2}	q_e (g/g)
0.2	0.10
0.4	0.13
0.6	0.15
0.8	0.16
1.0	0.17

In order to run over a range of conditions–notably, to run pure N_2 without CO_2 being artificially adsorbed–a simple continuous fit to Table 6 is used in MFIX-Exa of the form,

$$q_e = 0.17\, Y_{\text{CO}_2}^{0.3} \,. \tag{9}$$

It is strongly noted that Eq. (9) is not physically valid and should not be used outside of simulating these exact conditions.

A single monitor is used to calculate the (Lagrangian-) mean particle temperature. The adsorption response predicted by MFIX-Exa for the three conditions is compared to the experimental data[3] in Figure 9. The prediction is good, given the physics involved. In fact, the agreement is likely *too* good as the kinetics model has likely been over-fit for this specific set of operating conditions and not generally predictive outside of this very narrow envelope. It is notable that when cooling alone, i.e., as in Figure 8, MFIX-Exa under-predicts the cooling rate. Here, however, the cooling rate appears to be over-predicted. This discrepancy could point to deficiencies in the kinetics model, see discussion in Porcu et al. [15]. Finally, I note that there is some uncertainty in the inlet and wall boundary temperature which does have an impact on the predicted solution, see Figure 6.9 of Janssen [8].

Chapter 8: Conclusions

This report describes several bench-scale fluidization experiments that can be used to validate the CFD-DEM method as encapsulated in the MFIX-Exa code. The five cases considered are the cold-flow fluidized beds of Müller et al. [1, 2], Link et al. [3] (spout-fluid), and Goldschmidt et al. [4] (bi-disperse), the hot fluidized bed of Patil et al. [5, 6], and the adsorbing fluidized bed of Li et al. [7] and Janssen [8]. In most cases, MFIX-Exa with "standard" or "typical" CFD-DEM settings, the Gidaspow drag model, and the Gunn heat transfer provide a relatively good prediction of the quantities considered: mean void fraction profiles, mean velocity

[3]The experiments were replicated three times for each condition. There was non-negligible noise in the data and making it very difficult to distinguish individual curves in the published figures. Therefore, the data was digitized using an upper bound and lower bound envelope in an effort to capture the spread of the experimental data.

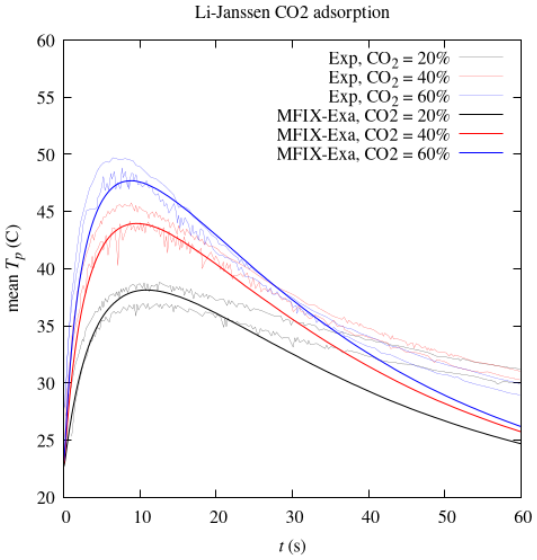

Figure 9: Comparison of mean particle temperature between MFIX-Exa simulation and the Li-Janssen experiment [8, 7].

profiles, fluctuating velocity profiles, mean particle temperature and segregation index. These results, with other verification and validation tests reported elsewhere, contribute to a body of work providing confidence and credibility in CFD predictions from the MFIX-Exa code.

Future work that is desired to do for this repository and report are summarized below.

- It would be worth investigating, at least in a one-off study, an alternative method of computing mean and standard deviation of particle velocity that is more in-line with the PEPT measurements in the Link case.
- Based on previous work [36, 32], prediction of the segregation index in the Goldschmidt bed should be improved with a polydisperse correction factor (PCF) [35]. It would be good to include a PCF drag law, at least through a user-defined function (UDF), to show that similar improvement is also observed here.
- Post-processing of the Goldschmidt case is slow because it uses a python script in serial to loop over all particle data in 60 plot files per simulation. This would be trivial (computationally) to do with a pair of monitors if the monitor functionality was extended to include filtering by type.
- The Patil and Li-Janssen cases assume a constant wall temperature. In reality, the wall will heat up and also hold some heat. It would be good to assess the impact of conjugate heat transfer on the cooling curves, especially in the Patil case. At the time of this writing, a conjugate convective heat transfer model is currently being developed and should be released to the community in the near future.
- While still staying with in the desired "one day turn-around" time, it would be nice to include larger cases, e.g., high particle counts. Similarly, it would be nice to include more complex cases, both geometrically, e.g., non-rectangular/non-cylindrical, and physically, e.g., actual chemical reactions.

Acknowledgments

This work would not have been possible at all without the support of the MFIX-Exa development team, past, present, and future. Further, Jordan Musser, Roberto Porcu, Deepak Rangarajan, and Aaron Lattanzi helped in originally setting up the case files used in this report. This work was performed in support of the U.S. Department of Energy's (DOE) Office of Fossil Energy's Advanced Energy Systems Multi-Year Research Plan (MYRP) through the National Energy Technology Laboratory (NETL) Research & Innovation Center's Simulation-Based Engineering (SBE) subprogram.

References

[1] Christoph R Müller, Daniel J Holland, Andrew J Sederman, Stuart A Scott, John S Dennis, and Lynn F Gladden. Granular temperature: comparison of magnetic resonance measurements with discrete element model simulations. *Powder Technology*, 184(2):241–253, 2008.

[2] Christoph R Müller, Stuart A Scott, Daniel J Holland, Belinda C Clarke, Andrew J Sederman, John S Dennis, and Lynn F Gladden. Validation of a discrete element model using magnetic resonance measurements. *Particuology*, 7(4):297–306, 2009.

[3] JM Link, NG Deen, JAM Kuipers, X Fan, A Ingram, DJ Parker, J Wood, and JPK Seville. PEPT and discrete particle simulation study of spout-fluid bed regimes. *AIChE journal*, 54(5):1189–1202, 2008.

[4] MJV Goldschmidt, JM Link, S Mellema, and JAM Kuipers. Digital image analysis measurements of bed expansion and segregation dynamics in dense gas-fluidised beds. *Powder Technology*, 138(2-3):135–159, 2003.

[5] A. V. Patil, E. A. J. F. Peters, and J. A. M. Kuipers. Comparison of CFD-DEM heat transfer simulations with infrared/visual measurements. *Chemical Engineering Journal*, 277:388–401, 2015.

[6] A. V. Patil, E. A. J. F. Peters, V. S. Sutkar, N. G. Deen, and J. A. M. Kuipers. A study of heat transfer in fluidized beds using an integrated dia/piv/ir technique. *Chemical Engineering Journal*, 259:90–106, 2015.

[7] Z. Li, T. C. E. Janssen, K. A. Buist, N. G. Deen, M. van Sint Annaland, and J. A. M. Kuipers. Experimental and simulation study of heat transfer in fluidized beds with heat production. *Chemical Engineering Journal*, 317:242–257, 2017.

[8] T. C. E. Janssen. *An investigation on heat transfer phenomena in fluidized bed reactors an experimental and modelling approach*. PhD thesis, Eindhoven University of Technology, 2015.

[9] Weiqun Zhang, Ann Almgren, Vince Beckner, John Bell, Johannes Blaschke, Cy Chan, Marcus Day, Brian Friesen, Kevin Gott, Daniel Graves, Max P. Katz, Andrew Myers, Tan Nguyen, Andrew Nonaka, Michele Rosso, Samuel Williams, and Michael Zingale. Amrex: a framework for block-structured adaptive mesh refinement. *Journal of Open Source Software*, 4(37):1370, 2019.

[10] Weiqun Zhang, Andrew Myers, Kevin Gott, Ann Almgren, and John Bell. Amrex: Block-structured adaptive mesh refinement for multiphysics applications. *The International Journal of High Performance Computing Applications*, 35(6):508–526, 2021.

[11] W.L. Oberkampf and C.J. Roy. *Verification and Validation in Scientific Computing*. Cambridge University Press, Cambridge, UK, 2010.

[12] P. J. Roache. *Verification and Validation in Computational Science and Engineering*. Hermosa Publisheres, Albuquerque, NM, 1998.

[13] William D Fullmer, Ann S Almgren, Michele Rosso, Johannes Blaschke, and Jordan Musser. Benchmarking of a preliminary mfix-exa code. *arXiv preprint arXiv:1909.02067*, 2019.

[14] Jordan Musser, Ann S Almgren, William D Fullmer, Oscar Antepara, John B Bell, Johannes Blaschke, Kevin Gott, Andrew Myers, Roberto Porcu, Deepak Rangarajan, Michele Rosso, Weiqun Zhang, and Madhava Syamlal. Mfix-exa: A path toward exascale CFD-DEM simulations. *The International Journal of High Performance Computing Applications*, 36(1):40–58, 2022.

[15] Roberto Porcu, Jordan Musser, Ann S Almgren, John B Bell, William D Fullmer, and Deepak Rangarajan. Mfix-exa: CFD-DEM simulations of thermodynamics and chemical reactions in multiphase flows. *Chemical Engineering Science*, 273:118614, 2023.

[16] Aaron M Lattanzi, William D Fullmer, Andrew Myers, and Jordan Musser. Toward polydisperse flows with mfix-exa. *Journal of Fluids Engineering*, 146(4), 2024.

[17] W. D. Fullmer, D. Rangarajan, and J. M. Musser. Dense granular flows with MFIX-Exa. Technical Report NETL-PUB-2025/4916, National Energy Technology Laboratory, Morgantown, WV USA, 2025.

[18] R. Cocco, W. D. Fullmer, P. Liu, and C. M. Hrenya. CFD-DEM: Modeling the small to understand the large. *Chemical Engineering Progress*, 113:38–45, 2017.

[19] William D Fullmer and Jordan Musser. CFD-DEM solution verification: Fixed-bed studies. *Powder Technology*, 339:760–764, 2018.

[20] D Lathouwers and J Bellan. Modeling of dense gas–solid reactive mixtures applied to biomass pyrolysis in a fluidized bed. *International Journal of Multiphase Flow*, 27(12):2155–2187, 2001.

[21] Jianmin Ding and Dimitri Gidaspow. A bubbling fluidization model using kinetic theory of granular flow. *AIChE Journal*, 36(4):523–538, 1990.

[22] C. Y. Wen and Y. H. Yu. Mechanics of fluidization. *Chemical Engineering Progress Symposium*, 62:100–111, 1966.

[23] Sabri Ergun. Fluid flow through packed columns. *Chemical Engineering Progress*, 48:89–94, 1952.

[24] DJ Gunn. Transfer of heat or mass to particles in fixed and fluidised beds. *International Journal of Heat and Mass Transfer*, 21(4):467–476, 1978.

[25] Peiyuan Liu, Casey Q LaMarche, Kevin M Kellogg, and Christine M Hrenya. Fine-particle defluidization: Interaction between cohesion, Young's modulus and static bed height. *Chemical Engineering Science*, 145:266–278, 2016.

[26] AB Morris, S Pannala, Z Ma, and CM Hrenya. Development of soft-sphere contact models for thermal heat conduction in granular flows. *AIChE Journal*, 62(12):4526–4535, 2016.

[27] J. Capecelatro and O. Desjardins. An euler-lagrange strategy for simulating particle-laden flows. *Journal of Computational Physics*, 238:1–31, 2013.

[28] J Shäfer, S Dippel, and DE Wolf. Force schemes in simulations of granular materials. *Journal de physique I*, 6(1):5–20, 1996.

[29] Leonardo E Silbert, Deniz Ertaş, Gary S Grest, Thomas C Halsey, Dov Levine, and Steven J Plimpton. Granular flow down an inclined plane: Bagnold scaling and rheology. *Physical Review E*, 64(5):051302, 2001.

[30] R. Garg, J. Galvin, T. Li, and S. Pannala. Documentation of open-source MFIX-DEM software for gas-solids flows. Technical report, National Energy Technology Laboratory, Morgantown, WV USA, 2012.

[31] Madhava Syamlal, Ismail Celik, and Sofiane Benyahia. Quantifying the uncertainty introduced by discretization and time-averaging in two-fluid model predictions. *AIChE Journal*, 63(12):5343–5360, 2017.

[32] Tingwen Li, Rahul Garg, Janine Galvin, and Sreekanth Pannala. Open-source MFIX-DEM software for gas-solids flows: Part ii–validation studies. *Powder Technology*, 220:138–150, 2012.

[33] Kun Luo, Junhua Tan, Zeli Wang, and Jianren Fan. Particle-resolved direct numerical simulation of gas–solid dynamics in experimental fluidized beds. *AIChE Journal*, 62(6):1917–1932, 2016.

[34] M.-S. Liou, L. Nguyen, C.-H. Chang, S. Sushchikh, R. Nourgaliev, and T. Theofanous. Hyperbolicity, discontinuities and numerics of two-fluid models. In H. Deconinck and E. Dick, editors, *Computational Fluid Dynamics*. Springer-Verlag, Berlin, 2006.

[35] R. Beetstra, M. A. van der Hoef, and J. A. M. Kuipers. Drag force of intermediate Reynolds number flow past mono- and bidisperse arrays of spheres. *AIChE Journal*, 53:489–501, 2007.

[36] M van Sint Annaland, GA Bokkers, MJV Goldschmidt, OO Olaofe, Martin Anton van der Hoef, and JAM Kuipers. Development of a multi-fluid model for poly-disperse dense gas-solid fluidised beds, Part II: segregation in binary particle mixtures. *Chemical Engineering Science*, 64(20):4237–4246, 2009.

[37] T.L. Dantas, F.M.T. Luna, I.J. Silva Jr, A.E. Torres, D.C.S. De Azevedo, A.E. Rodrigues, and R.F.P.M. Moreira. Modeling of the fixed-bed adsorption of carbon dioxide and a carbon dioxide-nitrogen mixture on zeolite 13x. *Brazilian Journal of Chemical Engineering*, 28(3):533–544, 2011.

U.S. DEPARTMENT of ENERGY

NATIONAL ENERGY TECHNOLOGY LABORATORY

Marianne Walck
Director
National Energy Technology Laboratory
U.S. Department of Energy

Marianne Walck (Acting)
Deputy Director & Chief Research Officer
Science & Technology Strategic Plans & Programs
National Energy Technology Laboratory
U.S. Department of Energy

Bryan Morreale
Associate Laboratory Director for Research & Innovation
Research & Innovation Center
National Energy Technology Laboratory
U.S. Department of Energy